# A pore-scale study of transport of inertial particles by water in porous media

*M.A. Endo Kokubun, A. Muntean, F.A. Radu, K. Kumar, I.S. Pop, E. Keilegavlen, K. Spildo*

UHasselt Computational Mathematics Preprint
Nr. UP-19-02

February 20, 2019

# A pore-scale study of transport of inertial particles by water in porous media

M. A. Endo Kokubun*[1], A. Muntean†[4], F.A. Radu‡[2], K. Kumar§[4], I.S. Pop¶[3], E. Keilegavlen‖[2], and K. Spildo**[1]

[1] *Department of Chemistry, University of Bergen, Norway*
[2] *Department of Mathematics, University of Bergen, Norway*
[3] *Faculty of Science, University of Hasselt, Belgium*
[4] *Department of Mathematics and Computer Science, University of Karlstad, Sweden*

**Abstract**

We study the transport of inertial particles in water flow in a porous medium. Our interest lies in understanding the accumulation of particles due to their inertia with respect to the water flow. The inhomogeneities caused by the tortuous paths in a porous medium can favour accumulation or dispersion of the particles in certain internal areas of the porous medium. We consider the particles as a dispersed phase immersed in the water phase, i.e, a fluid-fluid flow model, and assume Stokes drag as the momentum exchange between phases. Numerical simulations show that essentially two accumulation regimes can be identified: for low and high flow velocities. When particles accumulate at the entrance of a pore throat (high velocity region), the flow can be significantly modified, as the partial blockage of the pore causes a local redistribution of pressure. This redistribution can divert the upstream water flow into neighbouring pores. Moreover, we show that accumulation in high velocity regions occurs in heterogeneous media, but not in homogeneous media, where we refer to homogeneity with respect to the distribution of the pore throat diameters.

## 1 Introduction

The transport of particles in porous media emerge in many problems of interest, such as spillage of contaminants in soils [1, 2], water filtration systems [3], fines migration [4, 5],

*email: max.kokubun@uib.no
†email: adrian.muntean@kau.se
‡email: florin.radu@uib.no
§email: kundan.kumar@kau.se
¶email: sorin.pop@uhasselt.be
‖email: eirik.keilegavlen@uib.no
**email: kristine.spildo@uib.no

enhanced oil recovery [6, 7], to name a few. For enhanced oil recovery methods, injection of nanoparticles along with water has shown to recover initially trapped oil [8, 9, 10]. The enhancement can be an effect of a favourable change on the relative permeabilities curves [10] or improved mobility ratio [11], for example. These are effects of the interaction between the particles and water and/or oil. Another proposed mechanism is microscopic flow diversion [12, 13, 14]. This mechanism suggests that particles can accumulate when carried from a large to a narrow pore throat. If the accumulation is intense enough, the pore can clog, forcing the upstream flow into neighbouring channels. If the flow is diverted into a oil-containing channel, the initially-trapped oil may be recovered, thus enhancing recovery. In this case, the mechanism behind accumulation is particles inertia. This claim was supported by experimental results that shows that the enhancement in oil recovery is stronger in heterogeneous media, when compared to recovery in homogeneous media [15]. Here, we refer to homogeneity with respect to the pore size distribution. Therefore, heterogeneous media present more paths connecting large to narrow pores. Thus, it is expected that heterogeneous media exhibit a stronger enhancement in recovery if accumulation of particles due to inertia, and consequent flow diversion, is an important mechanism. Note that in this case the trapping mechanism occurs at the pore scale. At the reservoir scale, a different trapping mechanism can occur. For instance, at the transition zone between a high and a low-permeability regions, the difference in capillary pressures may trap the non-wetting phase in a two-phase flow [16, 17].

The transport of a particulate phase by a fluid phase has been studied for a long time. In the framework of Euler-Euler models, where the particulate phase is considered as a fluid phase as well, conservation equations for the evolution of particles concentration can be obtained through mixture theory [18, 19, 20]. Such models may take into account a large variety of effects: added-mass, drag, Basset history, particle collisions, etc. Often, closure relations must be provided that account for the mass and momentum transfer between phases. The need for such closure relations render difficulties in the treatment of the coupled phases. For very dilute mixtures, the so-called one-way coupled formulation is enough to describe the multiphase flow problem. In this case, the carrier fluid is not affected by the presence of the particles and can be fully determined independently. For increasing particles concentration, their volumetric occupation cannot be neglected, and one must consider a two-way coupled formulation [21]. When the particles concentration increases even further, the interparticle interaction must be considered, i.e., collisions, agglomeration and, in the case of droplets, break-up [22].

One-way coupled models have attracted quite some attention due to the rich behaviour they may present, even in the regime of dilute mixtures. It has long been recognized that particles which are heavier than the carrier fluid tend to accumulate in regions of dominating strain and disperse from regions of dominating vorticity [23, 24, 25]. Such feature have been proved useful for the study of particles carried by a turbulent flow field [26, 27, 28, 29]. For example, agglomeration of water droplets in preferential regions of a cloud, which presents turbulent convective currents, can lead to rain precipitation [30, 31]. Nevertheless, if the particulate phase is allowed to affect the carrier fluid phase, a two-way couple formulation must be considered, at least.

Flows established in porous media are highly heterogeneous at the pore scale due to the tortuous paths of the porous medium [32]. In fact, the non-homogeneities of the flow will

generate regions of dominating strain and/or vorticity inside the porous medium. With this in mind, we analyse the accumulation patterns that can occur for flow in random media. Our main focus is to evaluate whether particles accumulation can lead to partial clogging of a pore, thus diverting the upstream flow [33]. This is one of the proposed mechanism for enhanced oil recovery by polymer particles injection [15, 13]. For such, we need to consider a two-way coupled formulation, as one-way coupled models cannot capture the influence of the particulate phase on the carrier fluid. We will make use of a simple multiphase flow model that takes into account inertia of particles and the corresponding volumetric occupation. These are the minimum necessary physical effects that we must consider in order to observe particle accumulation and flow diversion. We also consider no interparticle interaction, thus avoiding the use of closure relations. Though restrictive, we proceed to show that the simple model is enough to shed light in the effect of accumulation.

We begin by introducing the multiphase flow model and present its dimensionless formulation. For the numerical simulations, we consider a porous medium consisting of non-overlapping solid circles distributed in a $2D$ rectangular box. We evaluate the influence of the parameters of interest: Stokes number, Reynolds number and particle-to-water densities mass ratio. Also, we show that the accumulation pattern is distinct if we consider a heterogeneous or a homogeneous media. In particular, the existence of clogs (accumulation in narrow pore throats, that may lead to flow diversion) only occurs in heterogeneous media.

# 2 Model formulation

We follow a general derivation based on the classical mixture theory [34, 35]. We consider that the solid phase is dispersed in the water phase, and hence, it can be described by a continuous field. The fractional volumetric occupation of the dispersed (solid) phase is given by $\phi \in [0, 1]$, whereas the water phase occupies a volumetric fraction of $1 - \phi$. We consider that the only internal interaction between the dispersed and the water phase is the Stokes drag. Additionally, if we consider that the pure mass densities of water and particles, $\rho$ and $\rho_p$, respectively, are constants, we have the following set of governing equations

$$\frac{\partial(1-\phi)}{\partial t} + \nabla \cdot ((1-\phi)\boldsymbol{u}) = 0, \tag{2.1}$$

$$\frac{\partial \phi}{\partial t} + \nabla \cdot (\phi \boldsymbol{v}) = 0, \tag{2.2}$$

$$\rho(1-\phi)\frac{D\boldsymbol{u}}{Dt} = -(1-\phi)\nabla p + \nabla \cdot ((1-\phi)\boldsymbol{\tau}_w) - \frac{\phi\rho_p}{t_s}(\boldsymbol{u}-\boldsymbol{v}), \tag{2.3}$$

$$\rho_p \phi \frac{d\boldsymbol{v}}{dt} = -\phi\nabla p + \frac{\phi\rho_p}{t_s}(\boldsymbol{u}-\boldsymbol{v}), \tag{2.4}$$

where $\boldsymbol{u}$ and $\boldsymbol{v}$ are the velocities of water and particles, respectively and $t_s = \rho_p d_p^2/(18\mu)$ is the Stokes time, or the characteristic response time of the particles with respect to changes in the flow field, with $d_p$ the particles diameter [20]. The stress tensor $\boldsymbol{\tau}_w$ of the water phase is given by

$$\boldsymbol{\tau}_w = \mu\left(\nabla\boldsymbol{u} + \nabla\boldsymbol{u}^T\right) - \frac{2}{3}\mu\boldsymbol{I}\nabla\cdot\boldsymbol{u}, \tag{2.5}$$

where $\mu$ is the dynamic viscosity of pure water. Moreover, we use the notation that

$$\frac{D}{Dt} = \frac{\partial}{\partial t} + \boldsymbol{u} \cdot \nabla, \quad \frac{d}{dt} = \frac{\partial}{\partial t} + \boldsymbol{v} \cdot \nabla, \tag{2.6}$$

are the material derivatives along the water and particles streamlines, respectively. Boundary and initial conditions will be added further ahead to complete the model.

The model given by Eqs. (2.1)–(2.4) assumes that the particles are small enough to not disturb the water flow locally. This means that we consider that there is no formation of wakes behind the particles. If the particles are big enough, vortices could be formed behind them, leading to a possible turbulence-generating mechanism. Formally, we consider that the particles diameter is such that the particle-based Reynolds number is smaller than one, i.e., $Re_p = \rho u_c d_p/\mu < 1$, where $u_c$ is some characteristic flow velocity. In other words, the flow around the particles is in the Stokes regime. Flows in porous media can exhibit a variation of several orders of magnitude in its velocity, typically from $1 - 100$ $\mu$m/s [36]. We are interested in inertial particles in the colloidal scale, i.e., $d_p \sim 10^{-4}$m, such that for water properties evaluated at $300K$, we have $Re_p \sim 10^{-6} - 10^{-4}$, typically. Therefore, for these conditions, transport of inertial particles in porous media will exhibit a Stokes flow around the particles. It is worth to note that even though the flow around the particles must be in the Stokes regime, the background flow does not have such restriction.

Equation (2.4), which governs momentum conservation for the dispersed phase, considers that the particles are rigid, non-deformable and do not interact with each other. This is analogous to consider the inviscid limit for the dispersed phase, thus neglecting the viscous contribution in the force balance at the right-hand side of Eq. (2.4). Moreover, this means that there is no additional pressure contribution due to particle collision, resulting that the pressure acts in both phases, only weighted by their respective volumetric occupation. More details can be seen in [19, 37]. Our goal here is to highlight two effects: that inertia of particles can lead to accumulation patterns for flows established in porous media, and that if the accumulation is large enough at the entrance of a pore throat, the flow can be diverted into a neighbouring pore. To reach this goal, we claim that (2.2)-(2.4), with proper initial and boundary conditions, is one of the simplest model that takes into account the processes leading to those two effects: inertia and volumetric occupation of particles.

The no-slip flow condition is considered for the water at the surface of the solid grains forming the porous medium. A question to be addressed regards the boundary condition of the particles velocity at the wall. The no-slip and no-flow conditions are not necessary true for particulate flow. For example, a perfect elastic collision would imply specular reflection, i.e., $[\boldsymbol{v} \cdot \boldsymbol{n}] = -2(\boldsymbol{v} \cdot \boldsymbol{n})\boldsymbol{n}$ and $[\boldsymbol{v} \cdot \boldsymbol{t}] = 0$, where $\boldsymbol{n}$ and $\boldsymbol{t}$ are the unitary vectors normal and tangential to solid boundaries, respectively. We will consider the limit of asymptotically small Stokes number, such that an explicit expression for $\boldsymbol{v}$ will be considered instead of Eq. (2.4). In this case, the particles velocity at the wall will be prescribed. The error in the calculation of the particle velocity at the wall introduced by this approximation is only relevant necessarily close to the wall.

## 2.1 Non-dimensionalization

We consider the following non-dimensional variables for a $2D$ geometry in the $(x, y)$ Cartesian coordinates

$$\hat{t} = t/t_c, \quad \hat{x} = x/l, \quad \hat{y} = y/l,$$
$$\hat{\boldsymbol{u}} = \boldsymbol{u}/u_c, \quad \hat{\boldsymbol{v}} = \boldsymbol{v}/u_c, \quad \hat{p} = p/p_c, \tag{2.7}$$

where $l$ and $u_c$ are characteristic values for length and velocity, with the characteristic time given by $t_c = l/u_c$, and $p_c = \mu u_c/l$ a characteristic pressure. The non-dimensional governing equations are then given by (we remove the hats for simplicity)

$$\nabla \cdot ((1-\phi)\boldsymbol{u} + \phi\boldsymbol{v}) = 0, \tag{2.8}$$

$$\frac{\partial \phi}{\partial t} + \nabla \cdot (\phi \boldsymbol{v}) = 0, \tag{2.9}$$

$$(1-\phi)\frac{D\boldsymbol{u}}{Dt} = -\frac{1}{Re}(1-\phi)\nabla p + \frac{1}{Re}\nabla \cdot \left((1-\phi)\left(\nabla \boldsymbol{u} + \nabla \boldsymbol{u}^T - \frac{2}{3}\boldsymbol{I}\nabla \cdot \boldsymbol{u}\right)\right) - \frac{\phi\tilde{\rho}}{St}(\boldsymbol{u} - \boldsymbol{v}), \tag{2.10}$$

$$\tilde{\rho}\frac{d\boldsymbol{v}}{dt} = -\frac{1}{Re}\nabla p + \frac{\tilde{\rho}}{St}(\boldsymbol{u} - \boldsymbol{v}), \tag{2.11}$$

where Eq. (2.8) was obtained by summing the dimensionless form of Eqs. (2.1) and (2.2) and we introduced the following dimensionless numbers

$$Re = \frac{\rho u_c l}{\mu}, \quad St = \frac{t_s}{t_c}, \quad \tilde{\rho} = \frac{\rho_p}{\rho}, \tag{2.12}$$

which are the Reynolds number, the Stokes number and the ratio of pure mass densities, respectively.

As mentioned previously, the model is limited by the constraint of a Stokes flow regime around the particles, i.e., $Re_p = \rho u_c d_p/\mu = Re(d_p/l) < 1$. Therefore, the Stokes regime around the particles is obeyed for $d_p/l < Re^{-1}$. Since $t_s = \rho_p d_p^2/(18\mu)$, we can write the Stokes number as $St = \tilde{\rho}(Re/18)(d_p/l)^2$. Then, we can write the constraint of Stokes regime around the spheres as

$$St < \frac{\tilde{\rho}}{18Re}. \tag{2.13}$$

## 2.2 Asymptotic limit of $St \ll 1$

In order to facilitate the analysis, we consider the asymptotic limit of small Stokes numbers, i.e., $St \ll 1$. This limit allows for a small response time of the particles with respect to changes in the surrounding flow field. In other words, the inertia effects are limited.

In this limit, we can expand the particles velocity in powers of $St$ as

$$\boldsymbol{v} = \boldsymbol{v}_0 + St\boldsymbol{v}_1 + o(St), \tag{2.14}$$

where $o(St)$ is interpreted as a Landau symbol. Using (2.14) into Eq. (2.11), which yields $d/dt = D/Dt + O(St)$, and equating the terms of order 0 and 1 in $St$ gives the following asymptotic expression for $\boldsymbol{v}$

$$\boldsymbol{v} = \boldsymbol{u} - St\left(\frac{1}{\tilde{\rho}Re}\nabla p + \frac{\partial \boldsymbol{u}}{\partial t} + \boldsymbol{u}\cdot\nabla\boldsymbol{u}\right) + o(St), \tag{2.15}$$

where it is required that $\tilde{\rho}Re > \mathcal{O}(St)$. Equation (2.15) is a modified version of the expression first obtained by Maxey [23] and used recently to study particle-laden turbulent flows [28, 27, 29, 38]. In the present case, we consider an additional contribution due to the pressure, and this difference is important for the near-wall treatment of particles velocity. Moreover, using $d/dt$ instead of $D/Dt$ allows for an explicit expression for $\boldsymbol{v}$, which facilitates the problem analysis, as will be shown ahead.

Using (2.15) we have the following system of governing equations

$$\nabla\cdot((1-\phi)\boldsymbol{u} + \phi\boldsymbol{v}) = 0, \tag{2.16}$$

$$\frac{\partial\phi}{\partial t} + \nabla\cdot(\phi\boldsymbol{v}) = 0, \tag{2.17}$$

$$(1-\phi)\frac{D\boldsymbol{u}}{Dt} = -\frac{1}{Re}(1-\phi)\nabla p + \frac{1}{Re}\nabla\cdot\left((1-\phi)\left(\nabla\boldsymbol{u} + \nabla\boldsymbol{u}^T - \frac{2}{3}\boldsymbol{I}\nabla\cdot\boldsymbol{u}\right)\right) - \frac{\phi\tilde{\rho}}{St}(\boldsymbol{u}-\boldsymbol{v}), \tag{2.18}$$

$$\boldsymbol{v} = \boldsymbol{u} - St\left(\frac{1}{\tilde{\rho}Re}\nabla p + \frac{\partial \boldsymbol{u}}{\partial t} + \boldsymbol{u}\cdot\nabla\boldsymbol{u}\right). \tag{2.19}$$

We can rewrite Eq. (2.17) as

$$\frac{1}{\phi}\frac{d\phi}{dt} = -\nabla\cdot\boldsymbol{v}, \tag{2.20}$$

where, as introduced previously, $d/dt$ is the material derivative along $\boldsymbol{v}$. Therefore, accumulation or dispersion of particles along its streamlines is characterized by the quantity

$$\nabla\cdot\boldsymbol{v} = \nabla\cdot\boldsymbol{u} - St\left(\frac{1}{\tilde{\rho}Re}\Delta P + \frac{\partial}{\partial t}\nabla\cdot\boldsymbol{u} + \nabla\cdot(\boldsymbol{u}\cdot\nabla\boldsymbol{u})\right). \tag{2.21}$$

According to Eqs. (2.20) and (2.21), when $\nabla\cdot\boldsymbol{v} < 0$, accumulation is favoured, whereas dispersion is favoured for $\nabla\cdot\boldsymbol{v} > 0$. Note that $\nabla\cdot\boldsymbol{u} \neq 0$ may happen in certain areas of the domain due to the inherent compressibility (see Eq. (2.16)).

We consider the no-slip flow for the water at the solid boundaries, i.e., $|\boldsymbol{u}| = 0$, at these boundaries. Therefore, Eq. (2.19) determines $\boldsymbol{v} = -St(\tilde{\rho}Re)^{-1}\nabla p$ as the particles velocity at solid boundaries. This condition implies slip flow and reflection of particles at the wall. The error introduced depends on which original boundary condition we had for the particles. For example, if we had specular reflection, the slip flow at the wall is unrealistic, but the reflection is not. Nevertheless, the error is restricted to the vicinity of solid boundaries. We will show that due to vorticity these regions are characterized by dispersion of particles, such that this error is not expected to be relevant.

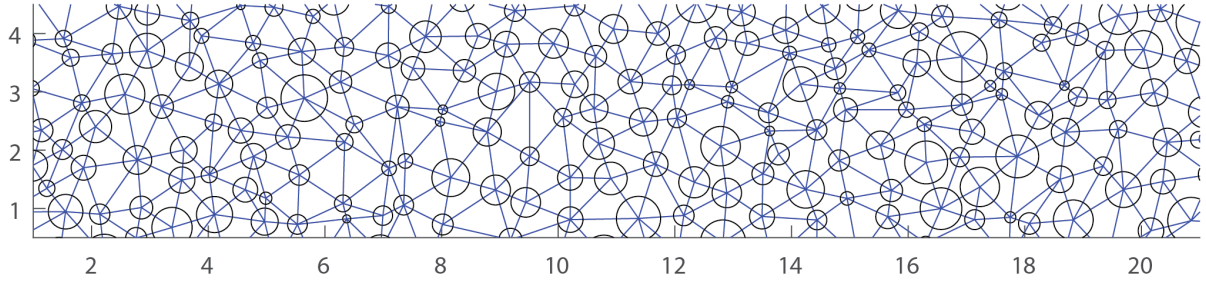


Figure 1: Illustrative porous medium. The nodes of the Delaunay triangulation provides the coordinates of the centres of the solid grains as well as the basis for calculating the pore throat diameters. The numerical domain comprises the void space between the solid grains (the mesh is not shown here).

# 3 Numerical results

The model given by Eqs. (2.16)–(2.19) will be solved in illustrative two-dimensional porous media. We will highlight the main features that arise in the accumulation patterns due to the non-homogeneity of the flow field established in the porous medium. Our intention is to quantify the behaviour of the model presented in the previous section in random media. We will consider media with given pore throat diameter distributions (PTDD). For such, first we establish a Delaunay triangulation in a $2D$ rectangle. We modify the distmesh algorithm [39] to perform the triangulation following a given distribution of edge lengths. The modified algorithm seeks a triangulation of the domain such that the edge lengths distribution follows the sum of two Gumbel distributions [40]

$$f_e(\lambda) = \sum_{i=1}^{2} \frac{1}{\beta_i} \exp\left(-z_i(\lambda) + e^{-z_i(\lambda)}\right), \tag{3.1}$$

where $\lambda$ are the values of the edge lengths and $z_i(\lambda) = (\lambda - \alpha_i)/\beta_i$. Then, we draw circles centred at each node of the triangles, making sure that circles do not overlap. Each pore throat diameter will be then given by subtracting from the length of the original triangle edge the radii of the circles located in its associated nodes. We construct the medium such that we can fit a bimodal distribution for the PTDD as a sum of two normal distributions

$$f_r(\xi) = \frac{p}{\sigma_1\sqrt{2\pi}} \exp\left(-\frac{(\xi-\eta_1)^2}{2\sigma_1^2}\right) + \frac{1-p}{\sigma_2\sqrt{2\pi}} \exp\left(-\frac{(\xi-\eta_2)^2}{2\sigma_2^2}\right), \tag{3.2}$$

where $\xi = \lambda - r_1 - r_2$ is the pore throat diameter length (with $r_1$ and $r_2$ the radii of the solid grains centred at the nodes of the edges $\lambda$), $\mu_i$ and $\sigma_i$ are the distribution parameters, with $i = 1, 2$, and $0 < p < 1$ the mixture probability. For convention, $\eta_1$ and $\sigma_1$ refers to the normal distribution around the smaller pores, whereas $\eta_2$ and $\sigma_2$ refers to the larger pores. The procedure is similar to the one described in [32].

We also define a parameter $\gamma$ as

$$\gamma = \frac{(1-p)\eta_2}{p\eta_1}, \tag{3.3}$$

which is a measurement of the large-to-narrow pore throat diameter ratio. For $\gamma \ll 1$, there is a predominance of smaller pores, whereas for $\gamma \gg 1$ there is a predominance of larger pores. For both limiting cases $\gamma \to 0$ and $\gamma \to \infty$, the medium is homogeneous.

We implement Eqs. (2.16)–(2.19) in COMSOL, thus numerically solving them using a fully coupled, standard Galerkin finite element method. The water velocity $\boldsymbol{u}$ is discretized using quadratic Lagrange elements, whereas the pressure $p$ and the volumetric fraction of particles $\phi$ are discretized using linear Lagrange elements. The system of equations is solved implicitly in a domain meshed by a Delaunay tesselation. We consider a parabolic injection profile for the water as $\boldsymbol{u} = (4u_{inj}(y - y_{min})(y_{max} - y)/(y_{max} - y_{min})^2, 0)$. The numerical domain will extend from $x \in [-1, 26]$ and $y \in [0.5, 4.5]$, but the solid grains fill the box $(1 \leq x \leq 21) \cup (0.5 \leq y \leq 4.5)$.

For numerical stability, we introduce an artificial diffusion term in Eq. (2.17), such that we essentially solve

$$\frac{\partial \phi}{\partial t} + \nabla \cdot \left( \phi \boldsymbol{v} - \frac{1}{Pe} \nabla \phi \right) = 0, \tag{3.4}$$

and we consider $Pe = 20$. It is worth to note that the artificial diffusion can be interpreted as particle diffusion in the water phase. Moreover, since $Pe > 0$, it tends to lower $\phi$, i.e., disperse particles concentration (see Eq. (2.21)). Nevertheless, as long as the advection transport is of unitary-order or lower, the influence of $Pe$ is very small, such that the role of diffusion will be restricted to numerical stabilization.

## 3.1 Illustrative results for heterogeneous and homogeneous media

We will begin by performing numerical simulations in the medium show in Fig. 1. This random medium is composed by 181 circles and pore throats. The parameters used for the initial edge lengths distribution are shown in Tab. 1.

| | |
|---|---|
| $\alpha_1 = 0.5$ | $\beta_1 = 0.05$ |
| $\alpha_2 = 0.8$ | $\beta_2 = 0.10$ |

Table 1: Parameters for the Gumbel distributions used to generate the Delaunay triangulation of the rectangular domain shown in Fig. 1.

This medium represents a heterogeneous porous medium with a PTDD shown in Fig. 2, where we plot the distribution of the pore throat diameters and the bimodal fit. For the distribution shown in Fig. 2, we have the fitting parameters shown in Tab. 2. We will consider $u_{inj} = 1.2, Re = 5, St = 0.1$ and $\tilde{\rho} = 10$. Note that according to (2.13), we must have $St < 0.11$ for the considered parameters. A value of $\tilde{\rho} = 10$ represent particles with a high mass density when compared to water, silver, for example.

| | |
|---|---|
| $p = 0.1834$ | $\gamma = 22.3662$ |
| $\eta_1 = 0.0842$ | $\eta_2 = 0.4232$ |
| $\sigma_1 = 0.0277$ | $\sigma_2 = 0.2191$ |

Table 2: Fitting parameters for the heterogeneous media shown in Fig. 1

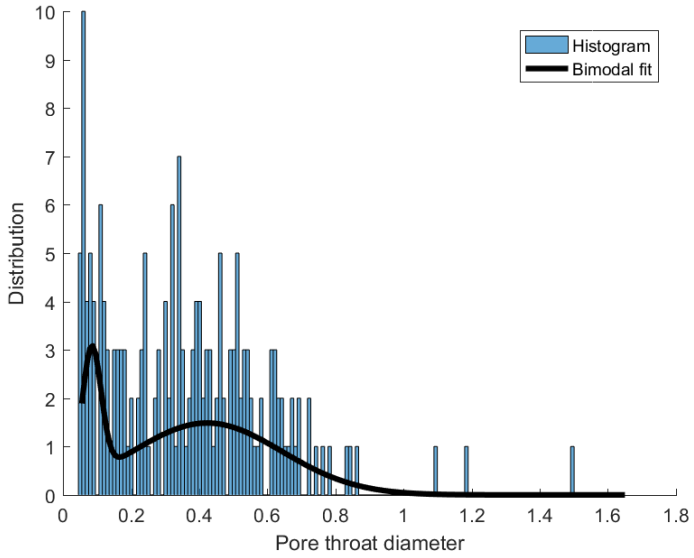


Figure 2: Bimodal distribution for the pore throat diameter of the medium shown in Fig. 1.

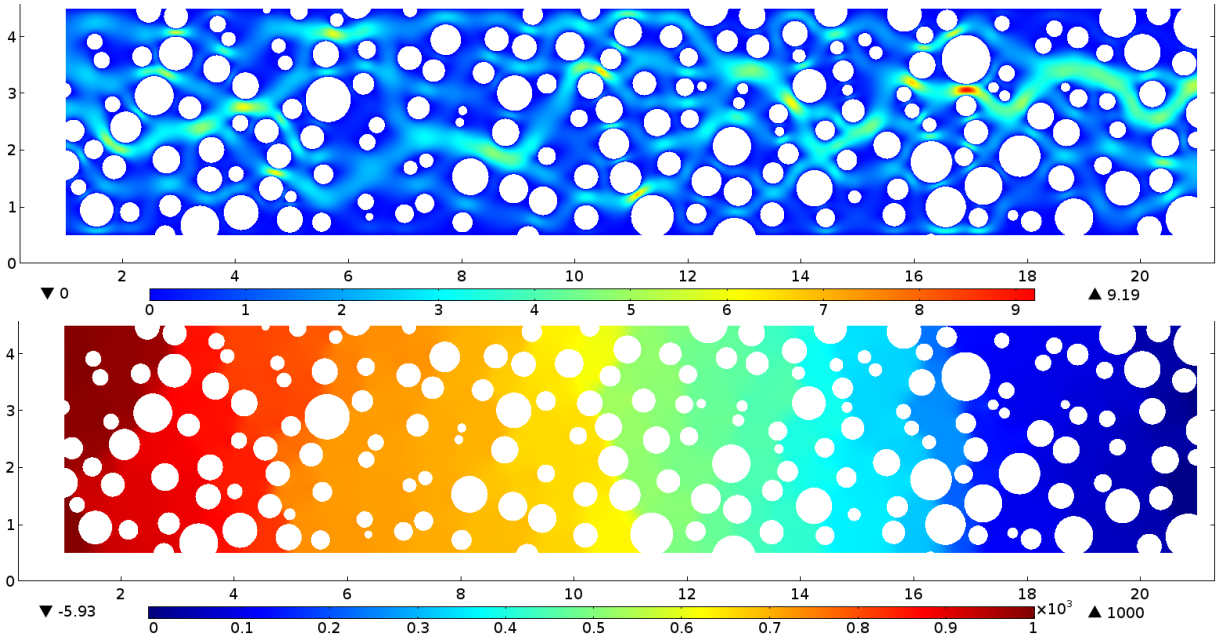


Figure 3: Flow pattern without particles ($\phi = 0$). Upper: Water phase velocity. Bottom: pressure drop along the domain. The flow is from left to right and shown for $t = 10$.

In Fig. 3 we show the water velocity field (upper) and the pressure drop (bottom) for the case of flow without particles, i.e., for $\phi = 0$ everywhere. The flow reached a stationary solution and it is shown at $t = 10$. One can see that the flow pattern is heterogeneous due to the tortuous paths of the porous medium. This heterogeneity in the velocity field is determinant for the accumulation and dispersion of particles. In fact, it is possible to predict regions where accumulation and dispersion will be predominant without solving the

full compressible model. To do so, we consider Eq. (2.21) with $\nabla \cdot \boldsymbol{u} = 0$, which happens when $\phi = 0$,

$$\nabla \cdot \boldsymbol{v} = -St \left( \frac{1}{\tilde{\rho} Re} \Delta p + \nabla \cdot (\boldsymbol{u} \cdot \nabla \boldsymbol{u}) \right). \tag{3.5}$$

Moreover, one can see that the pressure drop $\nabla p$ along the domain is nearly linear, such that $\Delta p \ll 1$. Hence, we expect that, quantitatively, the first term in the right-hand side of Eq. (3.5) is much smaller than the second term, such that we can approximate

$$\nabla \cdot \boldsymbol{v} \approx -St \left( \nabla \cdot (\boldsymbol{u} \cdot \nabla \boldsymbol{u}) \right) = -St \frac{(s^2 - w^2)}{2}, \tag{3.6}$$

where $s = \partial_y u_x + \partial_x u_y$ and $w = \partial_y u_x - \partial_x u_y$ are the local strain and vorticity of the flow, respectively. Of course, as particles tend to accumulate, compressibility effects will take place and (3.6) must be replaced by (2.21). Nevertheless, possible locations of accumulation and dispersion of particles can be estimated by analyzing (3.6) in the domain [28, 41, 21, 24].

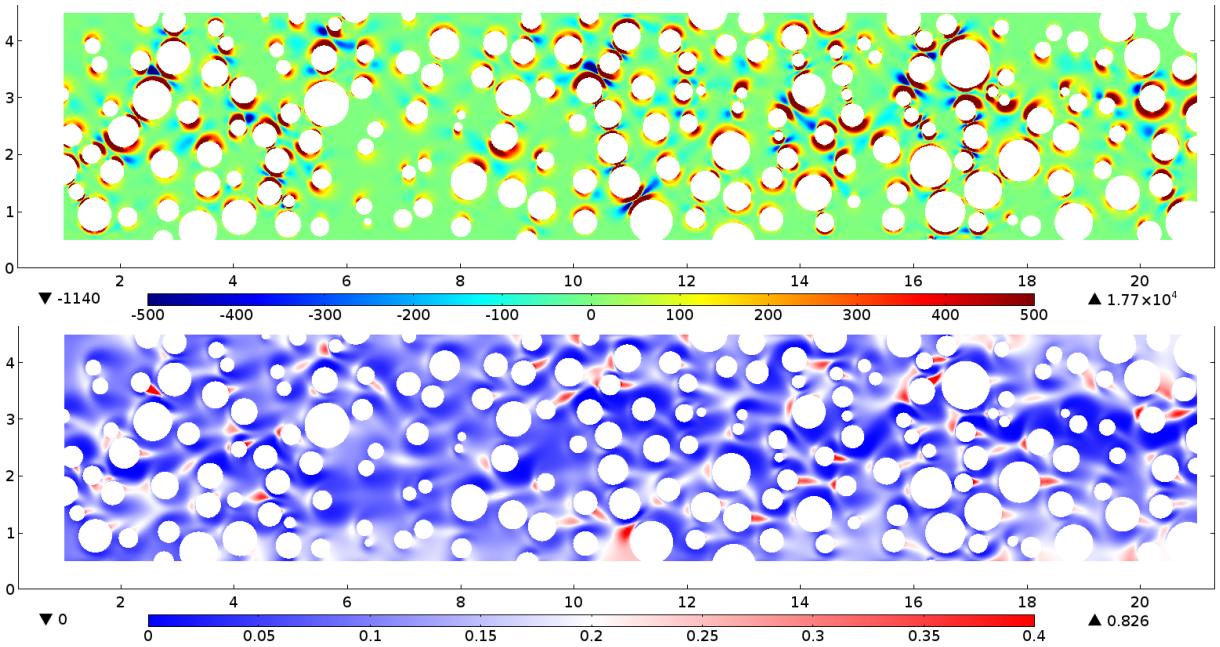


Figure 4: Upper part: surface plot of $-(s^2 - w^2)/2$. Regions where $-(s^2 - w^2)/2 < 0$ will tend to favour accumulation of particles, whereas regions where $-(s^2 - w^2)/2 > 0$ will favour dispersion. Bottom part: particles concentration for injection at $\phi = 0.1$. Plots are shown for $t = 80$, after the stationary regime was achieved.

In the upper part of Fig. 4, we plot $St^{-1} \nabla \cdot \boldsymbol{v} = -(s^2 - w^2)/2$. One can see that vorticity is induced near the solid boundaries of the circular grains, which will make particles disperse from it (positive regions in the upper Fig. 4). On the other hand, regions with dominating strain will favour accumulation, according to (3.6) and (2.20) (negative regions in the upper Fig. 4). The accumulation/dispersion pattern is shown in the bottom part of Fig. 4 by considering injection of particles with $\phi = 0.1$. Large rates of strain are caused by an abrupt change in the water velocity. In this scenario, one can recognize four different

characteristic regions where accumulation will be favoured: in the wake behind solid grains, at stagnation points, in no-flow regions near high-velocity regions and at the entrance of narrow pore throats. In Fig. 5 we show four zoomed-in regions from Fig. 4, each with a different characteristic particle accumulation pattern. We also plot the water streamlines as solid lines and particles velocity as arrows. Note that due to inertia, water and particles trajectories are not parallel.

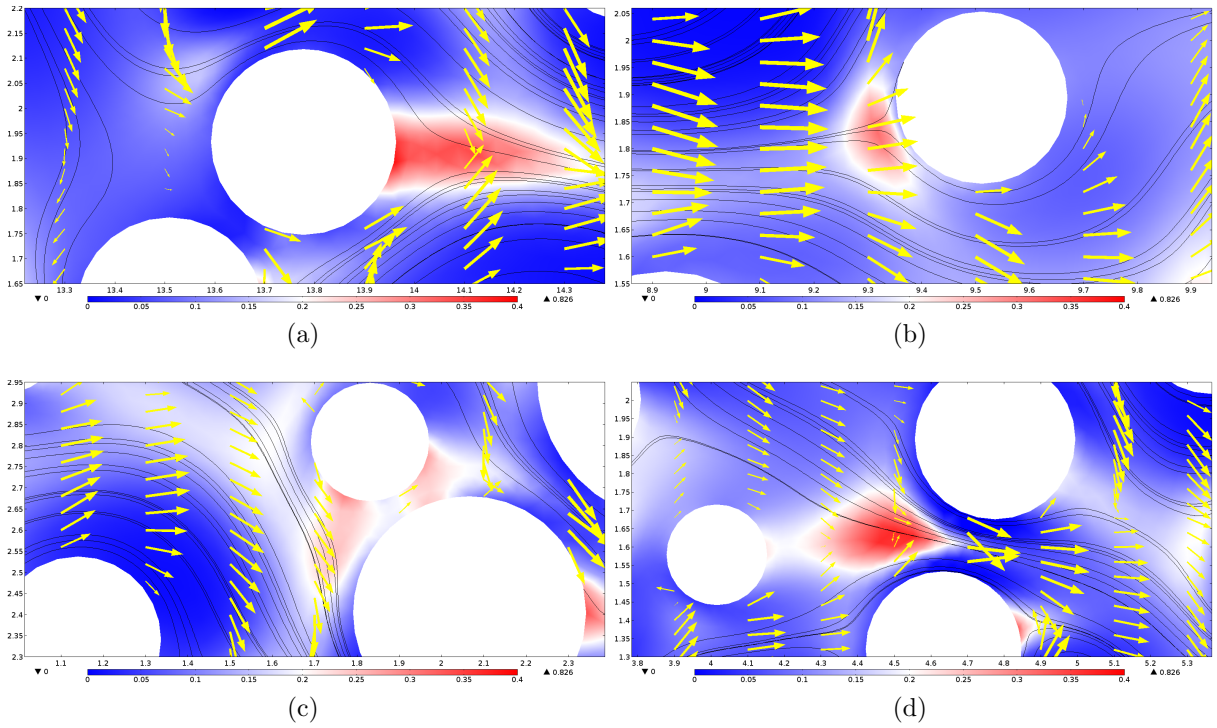

Figure 5: Particle concentration $\phi$ (surface plot), water streamlines (solid black lines) and particles streamlines (yellow arrows) for four different regions of the domain: (a) behind a solid grain, (b) at a stagnation point, (c) in a no-flow region and (d) at the entrance of a narrow pore throat.

From the four accumulation scenarios, only accumulation at the pore entrance, Fig. 5(d), can significantly alter the water flow. While in the other three cases the particles accumulate in a low-velocity region, at the pore entrance accumulation occurs in a high-velocity region. Therefore, if the accumulation capacity is large at the pore entrance, the channel may experience a partial or total clogging, which may causes a local redistribution of the pressure in the upstream side of the flow. If the clogging is severe, the local pressure redistribution can divert the water flow into neighbouring channels.

In Fig. 6 we show $p_{np} - p_p$, the pressure difference between the flow without particles and the flow with particles. The arrows in the domain point the clogs. One can see that in some regions of intense accumulation at the pore-entrance, the pressure decreased (larger positive values in Fig. 6), thereby causing the local pressure behind the channel to increase (negative values in Fig. 6). This can be more clearly seen in Fig. 7, where we show a zoomed-in

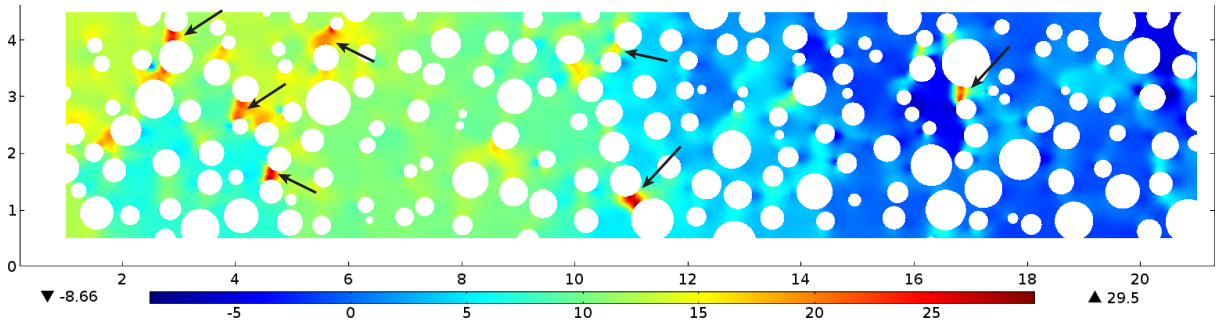


Figure 6: Pressure difference between the flow without and with particles. Positive regions means that the pressure decreased, whereas negative regions means that the pressure increased. The arrows point the clogs.

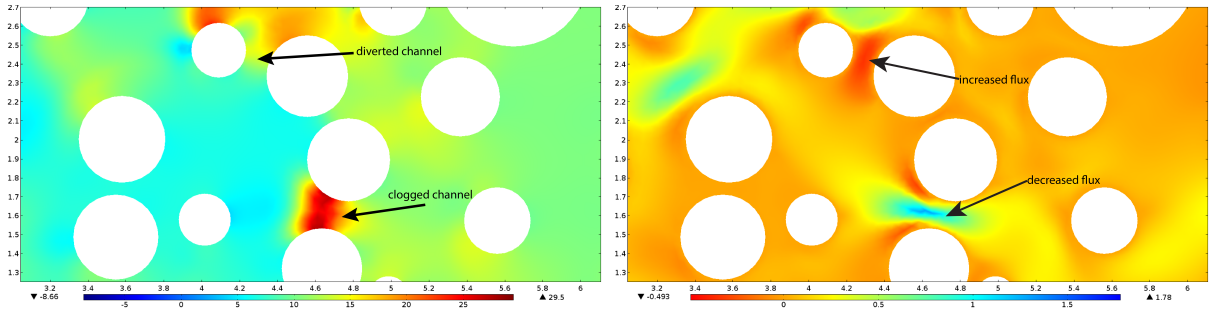


(a) (b)

Figure 7: Surface plot of the (a) pressure and (b) water flux differences between the cases without and with particles near a partially clogged channel.

region with the pressure difference and the difference between water fluxes divided by the average water flux in the case without particles, i.e., $(\Psi_{np} - \Psi_p)/\overline{\Psi}_{np}$, where $\Psi = (1-\phi)|\boldsymbol{u}|$ and $\overline{\Psi} = \Omega^{-1}\int_\Omega \Psi d\Omega$ is the average water flux in the domain $\Omega$. Note that at the entrance of the partially clogged channel, there is a pressure decrease. This happens because of the particle accumulation at the pore entrance, which decreases the water flow in the channel. Total clogging is not observed because in our model we do not consider particle attachment at the wall, and, by construction, our solid grains do not touch each other. Therefore, the region near the solid grain, which is dominated by vorticity, favours particle dispersion. One must bear in mind however, that due to the approximation (2.15) the error in $\boldsymbol{v}$ increases near the wall.

The occurrence of a clog can be identified by a pore throat presenting a significant decrease in the pressure at its entrance and a consequent decrease in its water flux. Since clogging is usually not complete, the near-wall regions of the partially clogged pore experience a faster flow, as discussed previously. Nevertheless, the overall water flux in the pore decreases, as we can see in Fig. 8, where we show the time variation of the water flux for the partially clogged channel and a nearby channel indicated in Fig. 7. Note that the decrease of the water flux in the partially clogged channel occurs at the same time scale as the increase

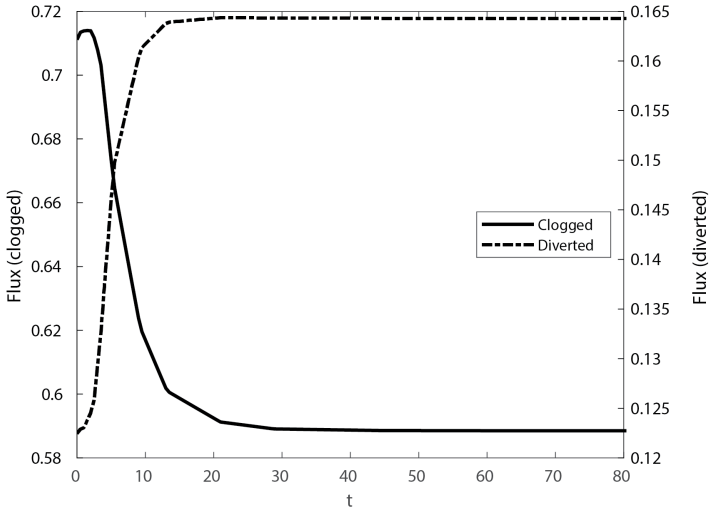


Figure 8: Time variation of the water flux $\Psi = (1-\phi)|\boldsymbol{u}|$ in the clogged and a nearby pore. Corresponding channels are indicated in Fig. 7(a).

in the water flux in the diverted channel. This indicates that these changes are correlated.

Since accumulation in a high velocity region is an effect of flow acceleration when going from a large to a narrow pore, it is expected that in a homogeneous medium this accumulation pattern is minimal, as most of the pores have the same size in such medium. To test this hypothesis, we consider a flow through the homogeneous medium shown in Fig. 10. For the initial edge lengths distribution, we use the same values shown in Tab. 1, only changing $\alpha_1 = 0.7$. This change was done to obtain a more homogeneous distribution of edges. After we draw the solid grains, the homogeneous medium have a PTDD shown in Fig. 9. We fit the PTDD through a bimodal distribution, with parameters given in Tab. 3.

| | |
|---|---|
| $p = 0.7289$ | $\gamma = 0.9235$ |
| $\eta_1 = 0.1350$ | $\eta_2 = 0.3352$ |
| $\sigma_1 = 0.0557$ | $\sigma_2 = 0.1400$ |

Table 3: Fitting parameters for the homogeneous media shown in Fig. 9

As discussed previously, it is expected that only significant accumulation at low-velocity regions will occur. Here, we consider the same parameters as before ($Re = 5, St = 0.1$ and $\tilde{\rho} = 10$), but now with injection of water occurring at $u_{inj} = 0.6$ [1]. In Fig. 10 we show surface plots for $St^{-1}\nabla \cdot \boldsymbol{v}$ and $\phi$. Note that we still have regions of predominant strain and vorticity. However, differently from what is observed for the heterogeneous medium (see Fig 4), the regions of dominating strain are mostly located in low-velocity regions. Therefore, an intense accumulation of particles occurs only in low-velocity regions, such that the flow pattern is not strongly modified by the accumulation of particles. This feature can be seen in Fig. 11, where, as before, we plot the pressure difference without and with particles.

[1] This modification on the injection condition was done in order to have values of $St^{-1}\nabla \cdot \boldsymbol{v}$ at the same order of magnitude as in the heterogeneous case, see upper part of Fig. 10.

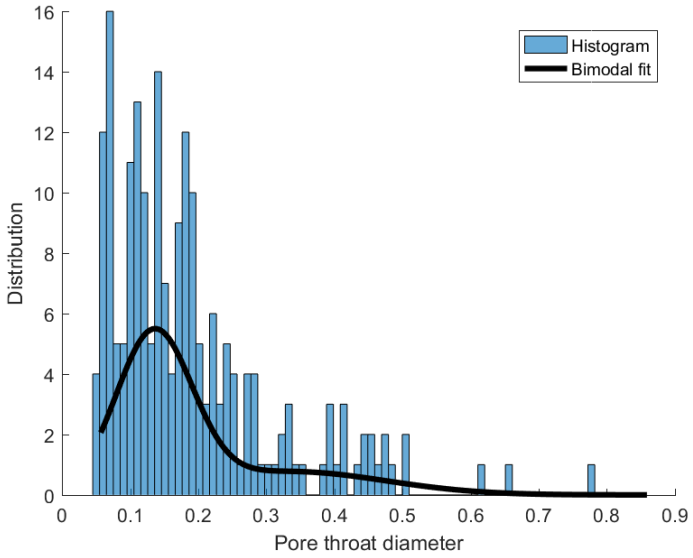


Figure 9: Pore throat diameter distribution of a homogeneous medium.

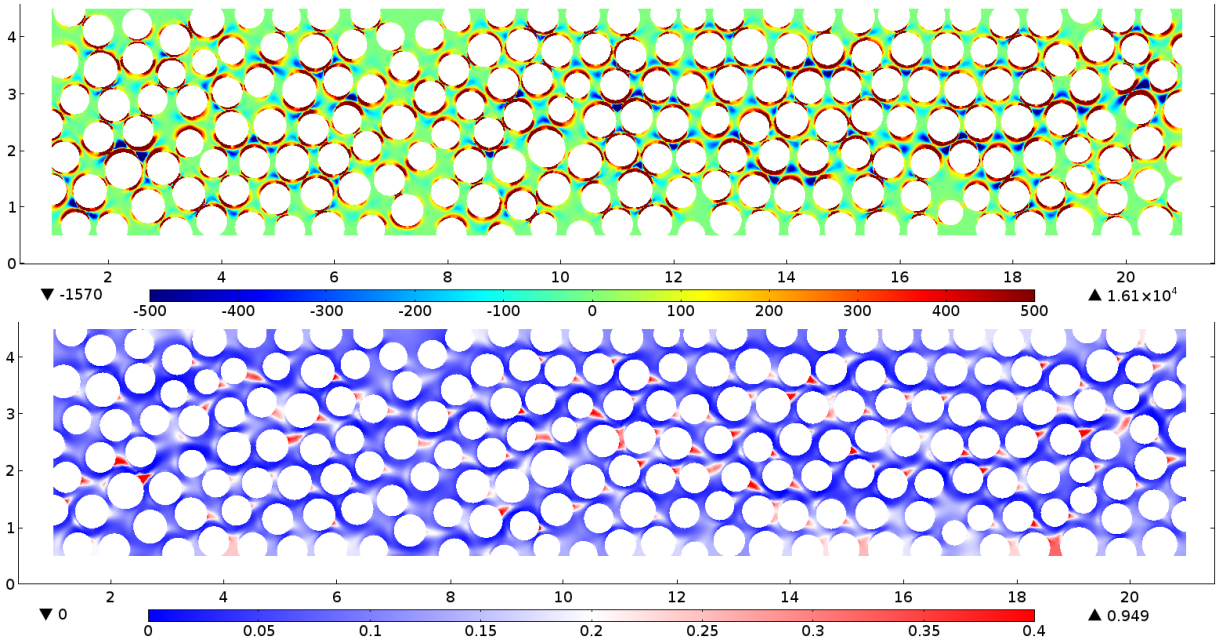


Figure 10: Upper part: surface plot of $-(s^2 - w^2)/2$. Bottom part: particles concentration for injection at $\phi = 0.1$.

The existence of higher accumulation in high-velocity regions only in heterogeneous media means that blockage of pores, with a consequent pressure redistribution in the upstream side and possible flow diversion, will not occur in homogeneous media. At least, not to a large extent. In the context of enhanced oil recovery through polymer particles injection, experimental results indicates that heterogeneous cores show increased rates of recovery compared to homogeneous cores [15]. These results are consistent with the proposed mechanism

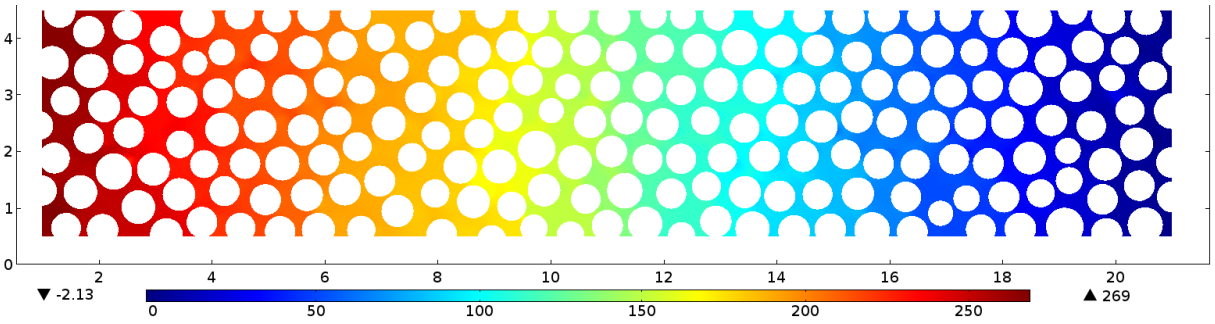


Figure 11: Pressure difference between the cases without and with particles. The linear decrease in the pressure is caused by the presence of particles in the flow and is not associated with partial blockage of pore channels.

of particle accumulation and flow diversion leading to EOR.

Note that the predominance of same-size pores will exist no matter which homogeneous medium we consider. Therefore, the lack of significant accumulation in high-velocity regions will be a feature of every homogeneous media, such that the conclusions drawn in this section are quite general. Formally, from our definition, homogeneous media are characterized by $\gamma \approx 0$ and $\gamma \gg 1$.

## 3.2 Influence of $u_{inj}$, $Re$ and $\tilde{\rho}$

As discussed in the previous section, accumulation and dispersion patterns can be analysed through the quantity $\nabla \cdot \boldsymbol{v}$. We showed that it is possible to evaluate this quantity in a flow scenario without particles in order to have an approximate relation between strain-dominated regions and accumulation, and between vorticity-dominated regions and dispersion. In our approach, the maximum accumulation will occur in the region where $\nabla \cdot \boldsymbol{v}$ achieves its minimal value. Therefore, by defining a parameter $\delta$ as

$$\delta = \min(St^{-1} \nabla \cdot \boldsymbol{v}) \tag{3.7}$$

we can study accumulation behaviour by analyzing the variations in it with the problem parameters. We will do so by considering the heterogeneous medium shown in Fig. 1.

For increasing values of the injection velocity $u_{inj}$ the rates of strain and vorticity through the medium increase. This leads to a decrease in $\delta$, as we can see in Fig. 12(a), where we plot $\delta$ for a fixed value of $Re = 5$. Therefore, for increasing injection velocities it is expected that accumulation increases. For a fixed value of $u_{inj}$ and varying values of $Re$, we have a non-monotonous variation of $\delta$, as shown in Fig. 12(b), where we consider $u_{inj} = \{1.0; 1.2; 1.4\}$. For small values of $Re$, an increase in the Reynolds number leads to an increase in $\delta$, thus lowering the accumulation of particles. However, after a critical $Re$, an increase in the Reynolds number leads to a decrease on $\delta$, thus enhancing accumulation of particles. An increase in $Re$ means a decrease on the viscous boundary layer at the solid grains surface. Since we keep the injection velocity fixed, an increase in $Re$ (and the consequent decrease on the viscous layer) means that the overall flow velocity increases. For the left branch, it means that an increase in the velocity leads to a decrease on the accumulation of particles,

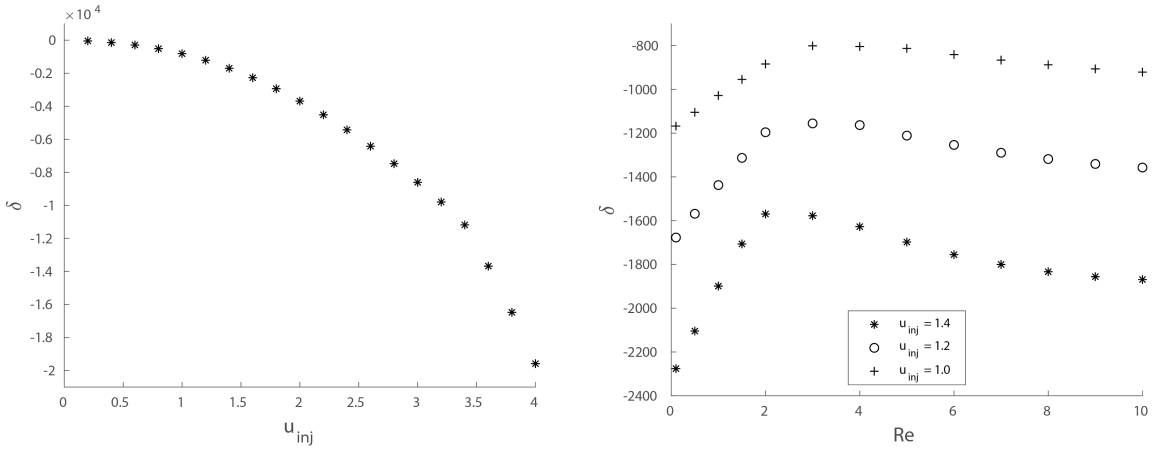


(a) (b)

Figure 12: (a) $\delta \times u_{inj}$ for $Re = 5$ and (b) $\delta \times Re$ for $u_{inj} = \{1.0, 1.2, 1.4\}$. Increasing values of the injection velocity leads to a decrease on $\delta$ and, consequently, on the accumulation rate. The variation with $Re$ presents two characteristic regimes: a Stokes regime (left branch) and a convection-dominated regime (right branch).

whereas for the right branch leads to an increase on the accumulation. We refer to the left branch as a Stokes regime and the right branch as a convection-dominated regime. Recalling that $\boldsymbol{v} \sim -\boldsymbol{u} \cdot \nabla \cdot \boldsymbol{u}$ and $\delta \sim -\nabla \cdot (\boldsymbol{u} \cdot \nabla \boldsymbol{u})$, we conclude that in the convection-dominated regime, accumulation and dispersion of particles is favoured by the increase in velocity. On the other hand, in the Stokes regime the convective transport is of higher-order, such that an increase in the velocity only enhances the transport of particles along with water. In fact, when $Re$ is small, the velocity of particles approximates as

$$\boldsymbol{v} \approx \boldsymbol{u} - \frac{St}{\tilde{\rho} Re} \nabla p, \tag{3.8}$$

such that $\nabla \cdot \boldsymbol{v} \approx \nabla \cdot \boldsymbol{u}$. Thus, in the Stokes regime, an increase on the overall flow velocity does not enhance accumulation. Rather, it decreases accumulation, as particles will be transported into the downstream direction. As shown in Fig. 12(b), the Stokes regime shrinks for increasing injection velocities, as expected.

As shown in (3.6), strain-dominated regions tend to favour accumulation. However, as pointed out by Eq. (2.20), this occurs along the streamlines of the particles. If the particles velocity increases considerably, accumulation locations might move further downstream inside the domain. For accumulation in low velocity regions, this poses a minor difference, as the particles streamlines are barely modified in such regions. On the other hand, for accumulation in high velocity regions, this will favour dispersion of particles, as they will tend to move further downstream, thus lowering accumulation. In Fig. 13 we plot the pressure difference for illustrative values of $\tilde{\rho} = 15, 10, 5$. A decrease in the particles-to-water mass densities ratio leads to an increase in the particles velocity, according to Eq. (2.19). We can see that the formation of clogs is unfavoured for decreasing values of $\tilde{\rho}$ (recalling that a clog is characterized by a significant decrease on the pressure at the pore entrance). If we write

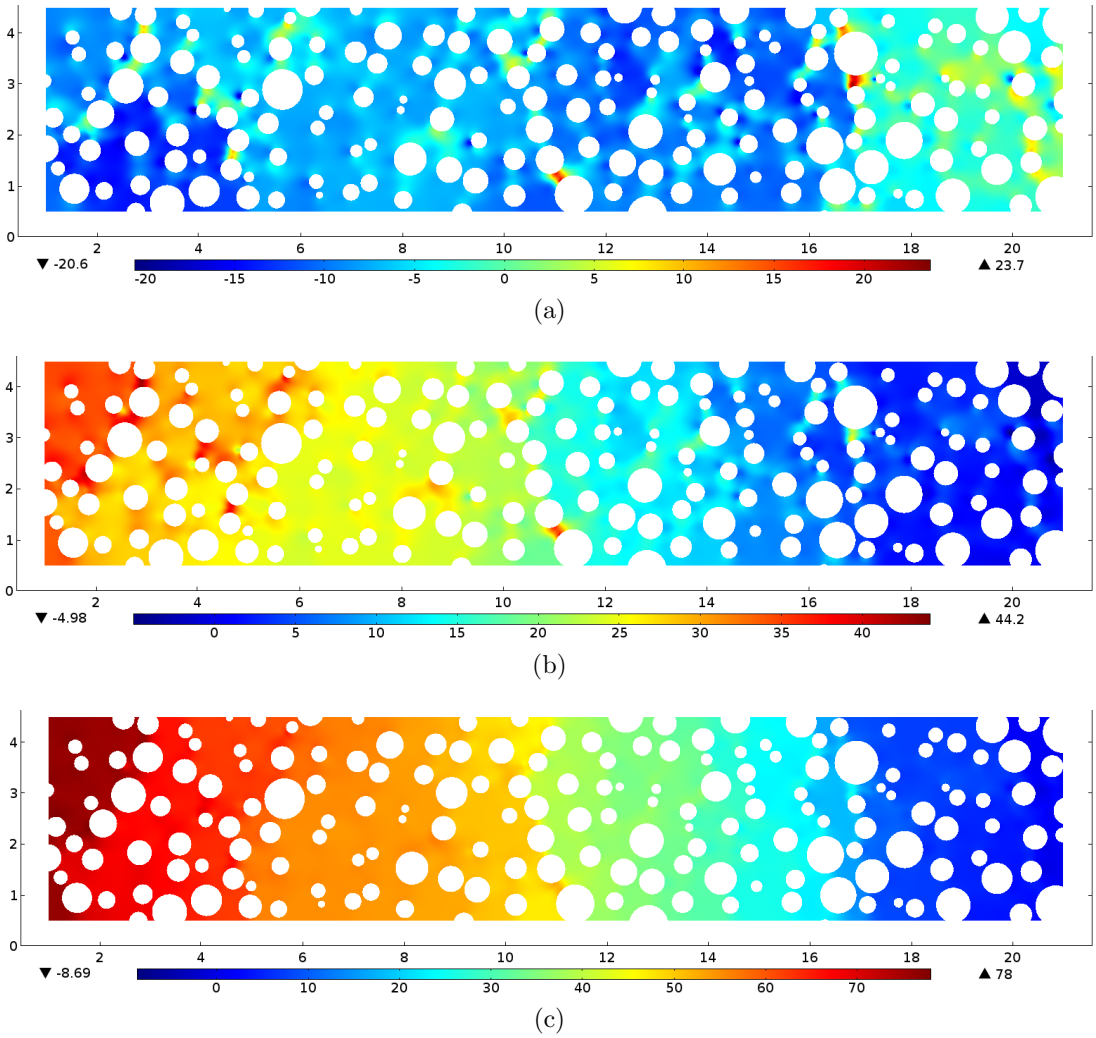


Figure 13: Pressure difference for (a) $\tilde{\rho} = 15$, (b) $\tilde{\rho} = 10$ and (c) $\tilde{\rho} = 5$. Decreasing values of $\tilde{\rho}$ increase the particles velocity $\boldsymbol{v}$ and favour the disappearance of clogs (recalling that clogs are characterized by an intense decrease on the pressure at the pore entrance).

Eq. (2.20) in Eulerian coordinates, we have

$$\frac{1}{\phi}\frac{\partial \phi}{\partial t} = -\nabla \cdot \boldsymbol{v} - \frac{1}{\phi}\boldsymbol{v} \cdot \nabla \phi. \tag{3.9}$$

Then, if we evaluate the local variation of $\phi$, we can see that particles with higher velocity tend to disperse accumulation due to the convective transport (second term in the right-hand side of Eq. (3.9)). This makes clogs disappear if the particles velocity is too high, as we can see in the surface plot of the pressure differences shown in Fig. 13.

# 4 Conclusions

We considered a simple multiphase flow model to analyse the transport of inertial particles by water in random media. The tortuous paths of the random medium generate regions of dominating strain and vorticity, which favours accumulation and dispersion of particles, respectively. The numerical results show that heterogeneous media present significant accumulation in low and high velocity regions, whereas homogeneous media present only significant accumulation in low velocity regions. Thus, blockage of pores and consequent redistribution of pressure on the upstream side occurs predominantly in heterogeneous media. This result supports the claim that particle accumulation and flow diversion plays a significant role in enhancing oil recovery through polymer particles, as proposed lately [15, 12, 13].

Detailed knowledge of the water flow pattern without particles in the porous medium can provide information as to where accumulation will be favoured by analysing strain-dominated regions. In the presence of particles, near the surface of the solid grains, vorticity is dominating and particles will tend to disperse from it. It is worth noting that stochasticity of real porous media is not perfectly described by circular grains. Therefore, more simulations should be performed for realistic media reconstructed from micro-CT scans from real rocks, for example.

As particles begin to accumulate, interparticle interaction should become relevant, such that a four-way coupled formulation must be considered [22]. In such scenario, the specification of the type of particle under consideration will be crucial. For example, some nanoparticles can form gels [42, 43] for increasing concentrations. For those particles, clogs will exhibit a snowball-like effect for increasing concentrations, possibly resulting in total clogging of a pore. Extending the model to account for the interactions of the particles requires the specification of the rheology of the particles.

# Acknowledgements

MAEK, EK and KS are supported by Equinor through the Akademia agreement. The work of AM is partially supported via MultiBarr (KK Foundation, project nr. 20180036). FAR was partially supported by the Norwegian Academy of Science and Letters and Equinor through the VISTA AdaSim project #6367. ISP was supported by the Research Foundation-Flanders (FWO) through the Odysseus programme (project GOG1316N) and by Equinor through the Akademia agreement. KK work was partially funded by the NFR Project 811716 LAB2FIELD.

# References

[1] J. McCarthy and J. Zachara, "Subsurface transport of contaminants," *Environmental Science and Technology*, vol. 23, pp. 496–502, 1989.

[2] A. Keller and M. Auset, "A review of visualization techniques of biocolloid transport processes at the pore scale under saturated and unsaturated conditions," *Advances in Water Resources*, vol. 30, pp. 1392–1407, 2007.

[3] M. Rezakazemi, A. Khajeh, and M. Mesbah, "Membrane filtration of wastewater from gas and oil production," *Environmental Chemistry Letters*, vol. 16, pp. 367–388, 2018.

[4] T. Russel and P. Bedrikovetsky, "Colloidal-suspension flows with delayed fines detachment: Analytical model and laboratory study," *Chemical Engineering Science*, vol. 190, pp. 98–109, 2018.

[5] L. Chequer and P. Bedrikovetsky, "Suspension-colloidal flow accompanied by detachment of oversatured and undersatured fines in porous media," *Chemical Engineering Science*, vol. 198, pp. 16–32, 2019.

[6] J. Mack and J. Smith, "In-depth colloidal dispersion gels improve oil recovery efficiency," *SPE 27780*, 1994.

[7] S. Borazjani, A. Behr, L. Genolet, A. Van Der Net, and P. Bedrikovetsky, "Effects of fines migration on low-salinity waterflooding: analytical modelling," *Transport in Porous Media*, vol. 116, pp. 213–249, 2017.

[8] Y. Li, "Oil recovery by low salinity water injection into a reservoir: a new study of tertiary oil recovery mechanism," *Transport in Porous Media*, vol. 90, pp. 333–362, 2011.

[9] M. El-Amin, S. Sun, and A. Salama, "Enhanced oil recovery by nanoparticles injection: modeling and simulation," *SPE 164333*, 2013.

[10] A. Zeinijahromi, R. Farajzadeh, H. Bruning, and P. Bedrikovetsky, "Effects of fines migration on oil-water relative permeability during two-phase flow in porous media," *Fuel*, vol. 176, pp. 222–236, 2016.

[11] J. Shi, A. Varavei, C. Huh, M. Delshad, K. Sepehrnoori, and X. Li, "Viscosity model of preformed microgels for conformance and mobility control," *Energy and Fuels*, vol. 25, pp. 5033–5037, 2011.

[12] K. Spildo, A. Skauge, and A. Skauge, "Propagation of colloidal dispersion gels (CDG) in laboratory corefloods," *SPE 129927*, 2010.

[13] M. Endo Kokubun, F. Radu, E. Keilegavlen, K. Kumar, and K. Spildo, "Transport of polymer particles in oil-water flow in porous media: enhancing oil recovery," *Transport in Porous Media*, vol. 126, pp. 501–519, 2019.

[14] S. Bolandtaba and A. Skauge, "Network modeling of EOR processes: a combined invasion percolation and dynamic model for mobilization of trapped oil," *Transport in Porous Media*, vol. 89, pp. 357–382, 2011.

[15] K. Spildo, A. Skauge, M. Aarra, and M. Tweheyo, "A new polymer application for North Sea reservoirs," *SPE 113460*, 2009.

[16] C. J. van Duijn, J. Molenaar, and M. J. de Neef, "The effect of capillary forces on immiscible two-phase flow in heterogeneous porous media," *Transport in Porous Media*, vol. 21, pp. 71–93, 2016.

[17] C. J. van Duijn, X. Cao, and I. S. Pop, "Two-Phase Flow in Porous Media: Dynamic Capillarity and Heterogeneous Media," *Transport in Porous Media*, vol. 114, pp. 283–308, 2016.

[18] R. Bowen, "The Theory of Mixtures," in *Continuum Physics, Volume III: Mixture and EM Field Theories* (A. Eringen, ed.), Academic Press, 1976.

[19] R. Jackson, "Locally averaged equations of motion of a mixture of identical spherical particles and a Newtonian fluid," *Chemical Engineering Science*, vol. 52, pp. 2457–2469, 1997.

[20] D. Gidaspow, *Multiphase Flow and Fluidization*. Academic Press, 1994.

[21] O. Druzhinin, "On the two-way interaction in two-dimensional particle-laden flows: the accumulation of particles and flow modification," *Journal of Fluid Mechanics*, vol. 297, pp. 49–76, 1995.

[22] S. Balachanda and J. K. Eaton, "Turbulent dispersed multiphase flow," *Annual Review of Fluid Mechanics*, vol. 42, pp. 111–133, 2010.

[23] M. Maxey, "The gravitational settling of aerosol particles in homogeneous turbulence and random flow fields," *Journal of Fluid Mechanics*, vol. 174, pp. 441–465, 1987.

[24] M. Maxey, "On the advection of spherical and non-spherical particles in a non-uniform flow," *Philosophical Transactions of the Royal Society A*, vol. 333, pp. 289–307, 1990.

[25] J. Fessler, J. Kulick, and E. J.K., "Preferential concentration of heavy particles in a turbulent channel flow," *Physics of Fluids*, vol. 6, p. 3742, 1994.

[26] T. Elperin, N. Kleeorin, V. L'vov, I. Rogachevskii, and D. Sokoloff, "Clustering instability of the spatial distribution of inertial particles in turbulent flows," *Physical Review E*, vol. 66, p. 036302, 2002.

[27] G. Falkovich and A. Pumir, "Intermittent distribution of heavy particles in a turbulent flow," *Physics of Fluids*, vol. 16, p. L47, 2004.

[28] G. Boffetta, A. Celani, F. De Lillo, and S. Musacchio, "The Eulerian description of dilute collisionless suspension," *Europhysics Letters*, vol. 78, 2007.

[29] D. Mitra and P. Perlekar, "Topology of two-dimensional turbulent flows of dust and gas," *Physical Review Fluids*, vol. 3, p. 044303, 2018.

[30] G. Falkovich, A. Fouxon, and M. Stepanov, "Acceleration of rain initiation by cloud turbulence," *Nature*, vol. 419, pp. 151–154, 2002.

[31] G. Falkovich and A. Pumir, "Sling effect in collisions of water droplets in turbulent clouds," *Journal of the Atmospheric Sciences*, vol. December, pp. 4497–4505, 2007.

[32] P. de Anna, B. Quaife, G. Biros, and R. Juanes, "Prediction of the low-velocity distribution from the pore structure in simple porous media," *Physical Review Fluids*, vol. 2, p. 124103, 2017.

[33] J. Su, G. Chai, L. Wang, w. Cao, Z. Gu, C. Chen, and X. Xu, "Pore-scale direct numerical simulation of particle transport in porous media," *Chemical Engineering Science*, 2019.

[34] S. Peker and S. Helvac, *Solid-liquid Two Phase Flow*. Elsevier, 2008.

[35] C. Kleinstreuer, *Two-phase Flow: Theory and Applications*. Taylor and Francis, 2003.

[36] Y. Kutsovsky, L. Scriven, H. Davis, and B. Hammer, "NMR imaging of velocity profiles and velocity distributions in bead packs," *Physics of Fluids*, vol. 8, p. 863, 1996.

[37] E. Guazzelli and O. Pouliquen, "Rheology of dense granular suspensions," *Journal of Fluid Mechanics*, vol. 852, p. P1, 2018.

[38] M. Esmaily-Moghadam and A. Mani, "Analysis of the clustering of inertial particles in turbulent flows," *Physical Review Fluids*, vol. 1, pp. 1–21, 2016.

[39] P.-O. Persson and G. Strang, "A simple mesh generator in MATLAB," *SIAM Review*, vol. 46, pp. 329–345, 2004.

[40] J. Lawless, *Statistical Models and Methods for Lifetime Data*. Wiley, 1982.

[41] Z. Dodin and T. Elperin, "On the motion of small heavy particles in an unsteady flow," *Physics of Fluids*, vol. 16, p. 3231, 2004.

[42] M. Bjørsvik, H. Høiland, and A. Skauge, "Formation of colloidal dispersion gels from aqueous polyacrylamide solutions," *Colloids and Surfaces A*, vol. 317, pp. 505–511, 2008.

[43] C. Marliere, P. Faure, P. Coussot, D. Vlassopoulos, A. Larsen, and B. Loppinet, "Jamming of Cellulose Ether Solutions in Porous Medium," *AIChE Journal*, vol. 61, pp. 3923–3935, 2015.

# UHasselt Computational Mathematics Preprint Series

## 2019

UP-19-02 *M.A. Endo Kokubun, A. Muntean, F.A. Radu, K. Kumar, I.S. Pop, E. Keilegavlen, K. Spildo*, **A pore-scale study of transport of inertial particles by water in porous media**, 2019

UP-19-01 *Carina Bringedal, Lars von Wolff, and Iuliu Sorin Pop*, **Phase field modeling of precipitation and dissolution processes in porous media: Upscaling and numerical experiments**, 2019

## 2018

UP-18-09 *David Landa-Marbán, Gunhild Bodtker, Kundan Kumar, Iuliu Sorin Pop, Florin Adrian Radu*, **An upscaled model for permeable biofilm in a thin channel and tube**, 2018

UP-18-08 *Vo Anh Khoa, Le Thi Phuong Ngoc, Nguyen Thanh Long*, **Existence, blow-up and exponential decay of solutions for a porous-elastic system with damping and source terms**, 2018

UP-18-07 *Vo Anh Khoa, Tran The Hung, Daniel Lesnic*, **Uniqueness result for an age-dependent reaction-diffusion problem**, 2018

UP-18-06 *Koondanibha Mitra, Iuliu Sorin Pop*, **A modified L-Scheme to solve nonlinear diffusion problems**, 2018

UP-18-05 *David Landa-Marban, Na Liu, Iuliu Sorin Pop, Kundan Kumar, Per Pettersson, Gunhild Bodtker, Tormod Skauge, Florin A. Radu*, **A pore-scale model for permeable biofilm: numerical simulations and laboratory experiments**, 2018

UP-18-04 *Florian List, Kundan Kumar, Iuliu Sorin Pop and Florin A. Radu*, **Rigorous upscaling of unsaturated flow in fractured porous media**, 2018

UP-18-03 *Koondanibha Mitra, Hans van Duijn*, **Wetting fronts in unsaturated porous media: the combined case of hysteresis and dynamic capillary**, 2018

UP-18-02 *Xiulei Cao, Koondanibha Mitra*, **Error estimates for a mixed finite element discretization of a two-phase porous media flow model with dynamic capillarity**, 2018

UP-18-01 *Klaus Kaiser, Jonas Zeifang, Jochen Schütz, Andrea Beck and Claus-Dieter Munz*, **Comparison of different splitting techniques for the isentropic Euler equations**, 2018

# 2017

UP-17-12 *Carina Bringedal, Tor Eldevik, Øystein Skagseth and Michael A. Spall*, **Structure and forcing of observed exchanges across the Greenland-Scotland Ridge**, 2017

UP-17-11 *Jakub Wiktor Both, Kundan Kumar, Jan Martin Nordbotten, Iuliu Sorin Pop and Florin Adrian Radu*, **Linear iterative schemes for doubly degenerate parabolic equations**, 2017

UP-17-10 *Carina Bringedal and Kundan Kumar*, **Effective behavior near clogging in upscaled equations for non-isothermal reactive porous media flow**, 2017

UP-17-09 *Alexander Jaust, Balthasar Reuter, Vadym Aizinger, Jochen Schütz and Peter Knabner*, **FESTUNG: A MATLAB / GNU Octave toolbox for the discontinuous Galerkin method. Part III: Hybridized discontinuous Galerkin (HDG) formulation**, 2017

UP-17-08 *David Seus, Koondanibha Mitra, Iuliu Sorin Pop, Florin Adrian Radu and Christian Rohde*, **A linear domain decomposition method for partially saturated flow in porous media**, 2017

UP-17-07 *Klaus Kaiser and Jochen Schütz*, **Asymptotic Error Analysis of an IMEX Runge-Kutta method**, 2017

UP-17-06 *Hans van Duijn, Koondanibha Mitra and Iuliu Sorin Pop*, **Travelling wave solutions for the Richards equation incorporating non-equilibrium effects in the capillarity pressure**, 2017

UP-17-05 *Hans van Duijn and Koondanibha Mitra*, **Hysteresis and Horizontal Redistribution in Porous Media**, 2017

UP-17-04 *Jonas Zeifang, Klaus Kaiser, Andrea Beck, Jochen Schütz and Claus-Dieter Munz*, **Efficient high-order discontinuous Galerkin computations of low Mach number flows**, 2017

UP-17-03 *Maikel Bosschaert, Sebastiaan Janssens and Yuri Kuznetsov*, **Switching to nonhyperbolic cycles from codim-2 bifurcations of equilibria in DDEs**, 2017

UP-17-02 *Jochen Schütz, David C. Seal and Alexander Jaust*, **Implicit multiderivative collocation solvers for linear partial differential equations with discontinuous Galerkin spatial discretizations**, 2017

UP-17-01 *Alexander Jaust and Jochen Schütz*, **General linear methods for time-dependent PDEs**, 2017

# 2016

UP-16-06 *Klaus Kaiser and Jochen Schütz*, **A high-order method for weakly compressible flows**, 2016

UP-16-05 *Stefan Karpinski, Iuliu Sorin Pop, Florin A. Radu*, **A hierarchical scale separation approach for the hybridized discontinuous Galerkin method**, 2016

UP-16-04 *Florin A. Radu, Kundan Kumar, Jan Martin Nordbotten, Iuliu Sorin Pop*, **Analysis of a linearization scheme for an interior penalty discontinuous Galerkin method for two phase flow in porous media with dynamic capillarity effects** , 2016

UP-16-03 *Sergey Alyaev, Eirik Keilegavlen, Jan Martin Nordbotten, Iuliu Sorin Pop*, **Fractal structures in freezing brine**, 2016

UP-16-02 *Klaus Kaiser, Jochen Schütz, Ruth Schöbel and Sebastian Noelle*, **A new stable splitting for the isentropic Euler equations**, 2016

UP-16-01 *Jochen Schütz and Vadym Aizinger*, **A hierarchical scale separation approach for the hybridized discontinuous Galerkin method**, 2016